Anomalous thermal effect in $ZrTe_5$ observed via photothermal measurements

Makoto Tsuneto,[1,*] Ran Jing,[1,2] Xinzhong Chen,[1] Sahal Kaushik,[1,3] Juntao Yao,[2,4] Dmitri E. Kharzeev,[1,5,6] Xu Du,[1] Qiang Li,[1,2] and Mengkun Liu[1,7,†]

[1] *Department of Physics and Astronomy, Stony Brook University, Stony Brook, New York 11794, USA*
[2] *Condensed Matter Physics and Materials Science Department, Brookhaven National Lab, Upton, New York 11973, USA*
[3] *Nordita, Stockholm University and KTH Royal Institute of Technology, SE-106 91 Stockholm, Sweden*
[4] *Department of Materials Science and Chemical Engineering, Stony Brook University, Stony Brook, New York 11794-3800, USA*
[5] *Department of Physics, Brook Haven National Laboratory, Upton, New York 11973-5000, USA*
[6] *RIKEN-BNL Research Center, Brook Haven National Laboratory, Upton, New York 11973-5000, USA*
[7] *National Synchrotron Light Source II, Brookhaven National Laboratory, Upton, New York, USA*

(Received 20 September 2023; revised 3 January 2024; accepted 19 January 2024; published 1 March 2024)

In this study, we explore the magnetothermoelectric power (MTP) of $ZrTe_5$, a canonical Dirac semimetal, through a photothermal technique. Unlike conventional thermoelectric studies that rely on on-chip heaters and are limited by fabrication processes, especially for stress-sensitive materials, our approach utilizes photothermal effects to induce temperature gradients. Our experiments, applying a magnetic field approximately parallel and transverse to the photocurrent detection direction, reveal that the photothermal method efficiently and reliably extracts both diagonal and off-diagonal components of the thermoelectric coefficient of $ZrTe_5$. We observe that the longitudinal MTP reproduces features previously reported in thermal transport studies, while the photoinduced transverse MTP confirms the anomalous Nernst effect. This photothermal measurement technique opens avenues for investigating transport properties in a wide range of quantum materials, in both three-dimensional and two-dimensional systems.

DOI: 10.1103/PhysRevApplied.21.034001

I. INTRODUCTION

In three-dimensional (3D) topological semimetals, such as Dirac semimetals [1,2] and Weyl semimetals [3,4], electrons near the conduction–valence-band crossing (Dirac point) behave as Dirac or Weyl fermions, which have left or right handedness, so-called "*chirality*" $\chi = \pm 1$ [1,3] ($\chi = \vec{p} \cdot \vec{\sigma}$ for massless particles, where $\vec{p}$ is the momentum vector and $\vec{\sigma} = (\sigma_x, \sigma_y)$ is the Pauli matrix). A particularly interesting phenomenon of these fermions is called chiral anomaly, where the symmetry of the left and right chirality is violated. The anomaly contributes to the chiral magnetic effect (CME) that a chiral charge current can be induced by a nontrivial arrangement of external fields, specifically parallel electric and magnetic fields [5,6]. The CME underpins a wide palette of new and exciting phenomena, such as near-dissipation-less charge transport [7], negative magnetoresistance (MR), and chiral magnetic photocurrents [8].

The CME has a magnetic field dependence. In the presence of coupling between chiral fermions and an electromagnetic field, gauge symmetry requires that chiral charge density, that is, the difference between the charge density of left- and right-handedness ($\rho_5 \equiv \rho_R - \rho_L$), changes with an external electric field parallel to the magnetic field [9]. With a finite static magnetic field, the conductivity has an additional contribution called chiral magnetic conductivity [5,6]:

$$\Delta\sigma^{zz}_{\mathrm{CME}} \propto B^2. \tag{1}$$

Here, the index zz denotes the longitudinal conductivity caused by the parallel electric and magnetic fields (along the direction of the fields). In other words, the CME manifests itself as an extra conductivity quadratic in the magnetic field, that is, negative MR. This phenomenon was measured in $ZrTe_5$ [10] and later in Na_3Bi [11], Cd_3As_2 [12,13], TaAs [14], NbAs [15], TaP [16], etc. According to the well-known Mott relationship [17], thermoelectric coefficients also acquire a characteristic field dependence at low fields. In such situations, the Mott formula relates $\Delta\sigma^{zz}_{\mathrm{CME}}$ and the (longitudinal) thermopower, S_{zz}. In the

*makoto.tsuneto@stonybrook.edu
†mengkun.liu@stonybrook.edu

leading order, S_{zz} depends on B^2 as follows [18]:

$$\frac{S_{zz}(B)}{S_{zz}(0)} = \left(1 - \frac{B^2}{B_0^2}\right)\left(1 + \frac{B^2}{B_0^2}\right)^{-1}. \quad (2)$$

For instance, the dc transport results for Cd_3As_2 with an on-chip heater are well fitted by Eqs. (1) and (2) [19]. Moreover, a recent study of $ZrTe_5$ further examined those anomalous behaviors in detail, showing that they were highly sensitive to the alignment of the magnetic field with the *a* axis [20].

$ZrTe_5$, as a 3D Dirac semimetal, has been shown to be a good platform for exploring many macroscopic quantum phenomena. Depending on the sample quality, $ZrTe_5$ experiences a Lifshitz transition at various temperatures, where the hole pocket at high temperature switches to an electron pocket at low temperature [21]. In the parallel electric and magnetic field configuration, $ZrTe_5$ exhibits the CME in the electronic and thermal transport measurements [10,19,22]. In the transverse electric and magnetic field configuration, both the anomalous Hall effect [23] and the anomalous Nernst effect [24] have been observed in single-crystal samples. The anomalous Hall effect remains in thin devices of $ZrTe_5$ [25]. In few-layer samples, integer quantum Hall effect (QHE) like behavior was reported, but the original claim of a 3D QHE was challenged by more recent experiments [26,27]. More intriguingly, $ZrTe_5$ can enter the quantum limit at low temperatures and low magnetic fields. At temperatures below 20 K, quantum oscillations can be observed in the electronic and thermal transport of $ZrTe_5$, and with only a few teslas, the electrons are confined in the lowest Landau level, and thus, the system enters the quantum limit [24,28,29].

Here, we use a focused laser beam rather than an on-device heater to induce a photothermal current in $ZrTe_5$. By taking advantage of the Shockly-Ramo (SR) formalism [30,31], we selectively measured the diagonal and off-diagonal components in the Seebeck coefficient. This study provides a convenient and alternative method to study thermal transport behavior, without the need for an on-device heating source. In our studies, we find that the magnetic field dependence of the diagonal and off-diagonal components of the thermoelectric coefficient reproduces nearly identical behavior to previously published results using the thermal transport method with on-device heaters.

II. METHODS

The samples studied in this work are flux-grown $ZrTe_5$ single crystals fixed on SiO_2/Si substrate, with fresh tape-cleaved surfaces. Four 100-nm-thick gold contacts were evaporated onto the sample through a shadow mask. The electrically wired samples are measured in a Quantum Design physical-property-measurement system for traditional electrical and thermal transport characterization. The photothermal measurement is performed in a high-vacuum optical cryostat with a magnetic field up to 7 T (Opticool, Quantum Design Inc.) The sample is elongated along the *a* axis. The contact configuration is displayed in the inset of Fig. 1(a). In the photothermal measurements, the *a* axis of the sample can be placed approximately parallel or transverse to the magnetic field. Magnetic-field-dependent dc transport measurements and photocurrent measurements can be performed with four-probe and two-probe schemes, respectively. To measure the photocurrent, we use a linearly polarized CO_2 laser ($\lambda \sim 10.6\ \mu$m) with a chopper frequency of 1 kHz. The incident power is 5 mW, and the focused beam size on the sample is tens of microns in width. The gap sizes between the two inner contacts are 20 to 100 μm, depending on the sample. Due to the thermal gradient created by the laser, the photocurrent is collected across the inner pair of electrodes and measured by a lock-in amplifier. The input impedance of the current-to-voltage preamplifier (60 Ω) is much larger than the sample resistance (<100 μΩ). Therefore, our photocurrent measurement directly scales with the Seebeck coefficient, and the sample resistance plays a negligible role. Noticeably, we observe no significant laser-polarization dependence of the photocurrent.

The theory of photothermal current collection has been well explained by the SR formalism [30–35]. The signal can be expressed as

$$I_{PC} = \int j_{PC} \cdot \nabla\phi_{SR} d^2r \propto \int \nabla T \cdot S \cdot \nabla\phi_{SR} d^2r,$$

where j_{PC} is the local photocurrent density generated by a thermal distribution, ∇T, multiplied by the Seebeck coefficient, S, and regulated by the overall resistance of the circuit. $\nabla\phi_{SR}$ is an auxiliary electric field established between the source and drain contacts, assuming they are at 0 and 1 V, respectively. In our experiments, the sample and contacts are prepared in regular square shapes, so that the auxiliary field always points straight from the drain to the source contact. With the SR formalism, we can measure one of the components in the Seebeck coefficient matrix by selectively aligning the magnetic field and beam spot.

III. RESULTS AND DISCUSSION

The dc resistance measurements are performed by the four-probe method with 1-μA current. As seen in Fig. 1(a), the resistance peaked around $T_p \sim 53$ K due to the change in its dominant carrier type due to the Lifshitz transition; this was consistent with previous measurements [21,36]. The measured T_p of our sample is lower than previously reported values [10,21,24,36–38], suggesting a lower defect concentration, and thus, good sample quality [21]. We first examined the Seebeck coefficient using thermal transport methods with the magnetic field along the *b* axis of the crystal. The Lifshitz transition of $ZrTe_5$ is manifested as a strong anomaly with or without magnetic fields

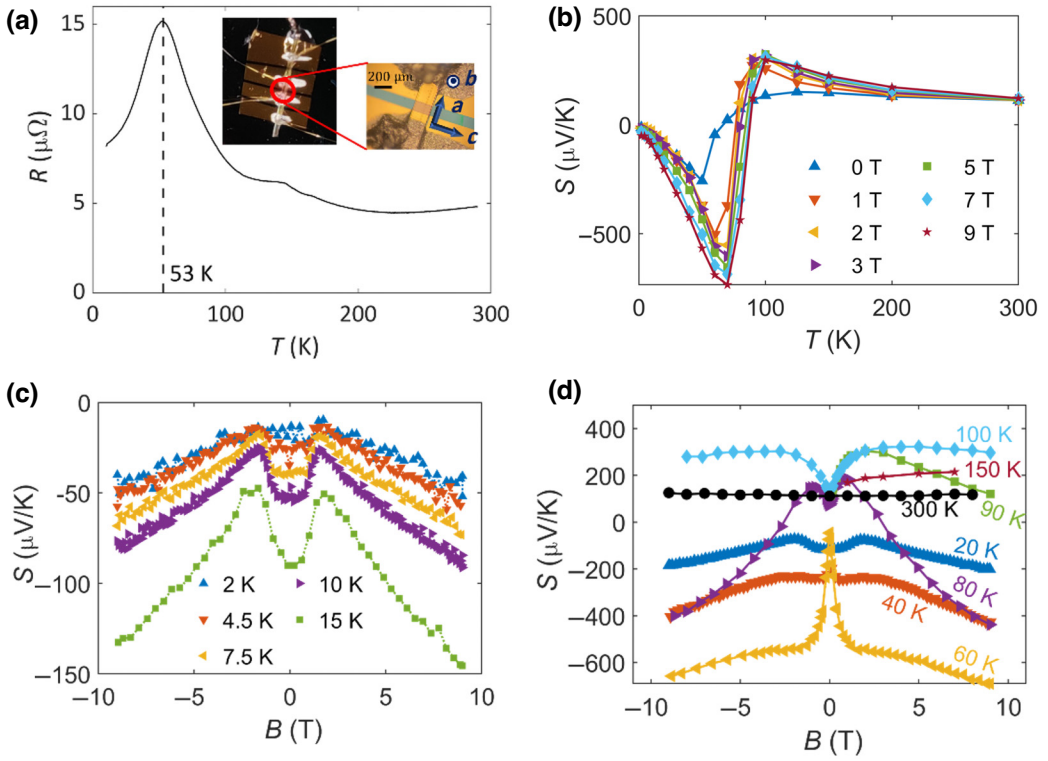

FIG. 1. Transport measurement geometry and results for $ZrTe_5$. (a) Result of dc transport measurements without a magnetic field. Inset, microscope images of our sample with gold electrodes. (b) Temperature dependence of the longitudinal Seebeck coefficient measured by the contact method. (c),(d) Magnetic field dependence of the longitudinal Seebeck coefficient at temperatures ranging from 2 to 300 K measured with the magnetic field aligned along the out-of-plane direction (along the *b* axis of the crystal).

between 50 and 70 K [Fig. 1(b)], consistent with previous results [21,23]. The sign-changing behavior is due to the switching of carrier type from holes above the transition to electrons below the transition. In Figs. 1(c) and 1(d), we summarize the magnetic field dependence of the Seebeck coefficient from 2 to 300 K measured by the thermal transport method with an on-chip heater. For data below 20 K [Fig. 1(c)], we observe a clear change of field dependence at around 2 T. The negative MR at low field can be explained by the weak antilocalization in Dirac semimetals induced by magnetic fields [39–41]. The MR changes to positive at high field. The absolute value of the Seebeck

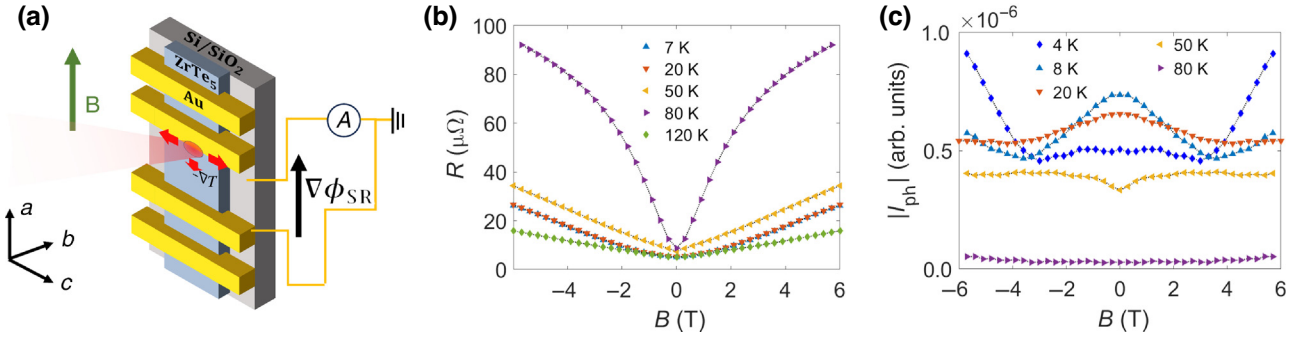

FIG. 2. Photothermal measurements of $ZrTe_5$ in a parallel electric and magnetic field configuration. (a) Schematic of the measurement. Magnetic field is aligned approximately along the *a* axis of the crystal. Laser is focused around one of the inner contacts. Thermal distribution of the laser spot, ∇T, generates the local photocurrent distribution. Photocurrent is collected by the two inner contacts. (b) MR measured in the configuration shown in (a). Positive MR indicates that the alignment of the magnetic field is not strictly along the electric field direction. (c) Magnetothermal photocurrent measured in the configuration shown in (a). Despite alignment of the magnetic field not being strictly in the parallel electric and magnetic field configuration, photocurrent signal shows a negative field dependence at low magnetic fields.

coefficient at a nonzero field gradually increases until 60 K [Fig. 1(d)] [21], beyond which the value quickly switches signs due to the Lifshitz transition. The transition behavior is consistent with our previous results on samples using identical preparation methods [18].

Now, we perform photothermal current measurements to extract the magnetic field dependence of the longitudinal component of the Seebeck coefficient. A schematic of the measurement is shown in Fig. 2(a). The magnetic field is aligned approximately parallel to the *a* axis of the crystal. The source and drain contacts are also aligned with the *a* axis. The MR of our sample is displayed in Fig. 2(b). The result did not show negative MR due to a small misalignment of the sample's *a* axis with the magnetic field. As shown in Fig. 2(a), we focus the laser-beam spot around one of the inner contacts. The laser generates a thermal distribution, and consequently, a photocurrent distribution on the sample surface. The local photocurrent distribution generated along the *c* and *b* axes of the crystal does not contribute to the acquired current because the auxiliary field defined in the SR formalism aligns from the drain to the source (along the *a* axis). The only contributing local term is $j_{\mathrm{PC},a} \propto S_{aa}\partial_a T$, and thus, the collected nonlocal signal is $I_{\mathrm{PC}} \propto S_{aa}(B)$. In Fig. 2(c), we show the acquired magnetothermoelectric power (MTP). We observe a negative magnetic field dependence of the photothermal signal at low field and a switch to positive dependence at 3–4 T below 20 K. This behavior is absent in our data above 50 K. Together with the positive MR, we reproduce identical features of the published results [20] with a 3° misalignment of the magnetic field. We note that our sample is also flux grown. According to Ref. [20], the crystal growth method may influence the electron behavior of $ZrTe_5$, which is assumed to be critical for understanding the MR and MTP behavior at low temperatures. The samples used in both experiments also share similar Lifshitz transition temperatures, indicating that the reproduction of identical magnetothermoelectric behavior is reliable.

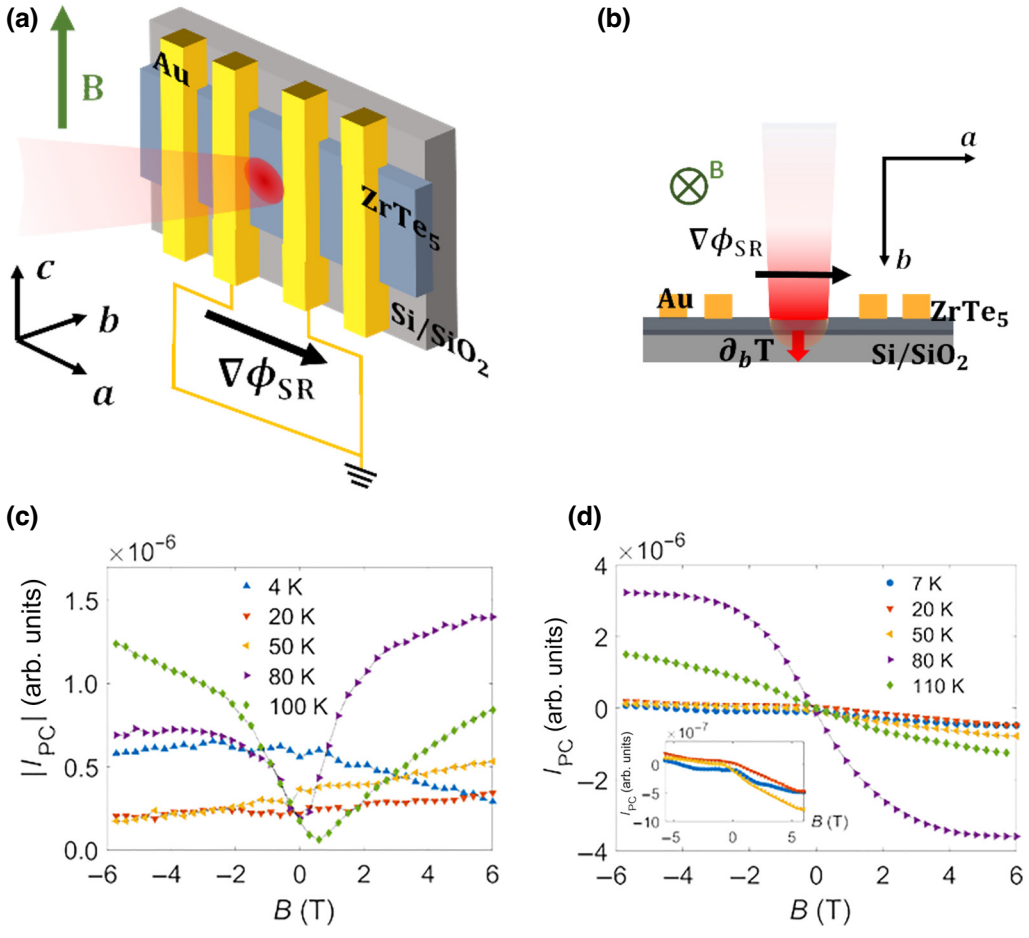

FIG. 3. Photothermal measurements with a magnetic field perpendicular to the *a* axis of the crystal. (a) Experimental schematics with axes definition. (b) Side view of the schematics to characterize the direction of field *B*, thermal gradient ∇T, and current $\nabla\phi_{\mathrm{SR}}$. (c) In general cases, both signals symmetric and antisymmetric to the magnetic field contribute to the photocurrent measurement. (d) By carefully aligning the laser spot to the center point between two contacts, the symmetric component can be removed, and the signal is solely contributed to by the transverse component of the thermoelectric coefficient.

According to finite-element-method simulations with COMSOL Multiphysics using an a-axis thermal conductivity of $\kappa_a \sim 50$ W/(m K) at 4 K, and beam width of about 70 μm, the temperature difference between two electrodes is found to be about 0.1 K. These results confirm that the photothermal method can faithfully extract the longitudinal MTP.

Next, we demonstrate the photothermal current results with the in-plane magnetic field aligned with the c axis to extract the magnetic field dependence of the Nernst coefficient [Fig. 3(a)]. Unlike in the previous measurement, we adjust the focusing spot of the laser to the middle point of two inner contacts. The laser generates thermal distributions in both the in-plane and out-of-plane directions [Figs. 3(a) and side view in 3(b)]. In this configuration, because the magnetic field is aligned in plane, the auxiliary field defined in the SR formalism still points straight from the drain to the source contact. The local current flowing in the c- and b-axis directions does not contribute to the signal. The remaining contributing term is $j_{\mathrm{PC},a} \propto -S_{ba}\partial_b T + S_{aa}\partial_a T$. The S_{ba} contribution is antisymmetric to the magnetic field, whereas the S_{aa} contribution is symmetric. Without too much adjustment, we can readily observe the sum of both signals, as shown in Fig. 3(c). We note that the in-plane (a-c plane) thermal gradient can generate an in-plane photocurrent along both the $+a$ and $-a$ directions. Therefore, by carefully adjusting the position of the illumination spot, the integration of the longitudinal contribution can be zero. In our simple sample configuration, we align the beam spot to the middle point between two contacts to make sure the S_{aa} contribution (symmetric in the magnetic field) is always zero. The remaining S_{ba} component has zero signal at $B = 0$, as shown in Fig. 3(d). The contribution from S_{ba} depends on the thermal gradient along the out-of-plane ($\partial_b T$) direction, as shown in Fig. 3(b). The sign of the gradient does not depend on where the photocurrent is generated. Therefore, the S_{ba} term is not canceled upon integration. As expected, our data in Fig. 3(d) show that the photothermal signal, $I_{\mathrm{PC}} \propto S_{ba}(B)$, is antisymmetric in B (80, 110 K).

The saturating behavior of the transverse component of the MTP indicates an anomalous Nernst effect. The normal Drude-like Nernst coefficient, $S^N_{ba}(B)$, decays to zero at high field, while the anomalous Nerst coefficient, $S^A_{ba}(B)$, saturates to a finite value. They can be approximated as

$$S^N_{ba}(B) = S^N_0 \frac{\mu B}{1 + (\mu B)^2}, \tag{3}$$

$$S^A_{ba}(B) = \Delta S^A_{ba} \tanh\left(\frac{B}{B_0}\right), \tag{4}$$

respectively [18,42]. Here, μ and B_0 are the charge mobility and the field where the anomalous effect saturates. S^N_0 and ΔS^A_{ba} denote the amplitudes of conventional and anomalous components of the Nernst effect, respectively. At high field, we observe a saturating Nernst effect rather than vanishing behavior at all temperature points investigated below 100 K, supporting the existence of anomalous thermoelectric effects [24]. Interestingly, at the base temperature of the experiment, 7 K, we observe weak quantum oscillation behavior arising from Landau bands. Compared with previous thermal transport results [24], the oscillation amplitude is weaker at similar temperatures, which is likely to be due to the heating effect of the 5-mW illumination on the sample surface.

IV. CONCLUSION

In this work, we investigated the magnetothermoelectric power of the 3D Dirac semimetal $ZrTe_5$. Instead of using canonical thermal transport techniques, we take advantage of the photothermal effect to induce local photocurrent density. Due to the simple geometry of the sample and contact configuration, we can selectively acquire the longitudinal and transverse components of the MTP. In the approximately parallel electric and magnetic field regime, our photothermal measurements reproduce nearly identical features to the result acquired from thermal transport measurements with an estimated 3° misalignment of the magnetic field [20]. In the transverse magnetic field regime, we measure the Nernst thermopower. The saturation behavior at high magnetic fields is consistent with the anomalous Nernst effect previously observed in canonical thermal transport measurements. Our study highlights that the photothermal experiment serves as a convenient and reliable method to study the thermoelectric behavior of bulk samples. This technique can also be broadly applied to thin films, thin crystals, and two-dimensional materials.

ACKNOWLEDGMENTS

This work at Brookhaven National Laboratory (BNL) was supported by the U.S. Department of Energy, Office of Basic Energy Sciences, Division of Materials Sciences and Engineering, under Contract No. DE-SC0012704. This research used resources of the Center for Functional Nanomaterials, which is a U.S. DOE Office of Science Facility, at BNL. X.D. acknowledges support from the National Science Foundation (NSF) under Grant No. DMR-1808491. Nordita is supported in part by NordForsk. The authors acknowledge the valuable discussion with Dr. Bing Chen.

[1] Z. Wang, Y. Sun, X. Q. Chen, C. Franchini, G. Xu, H. Weng, X. Dai, and Z. Fang, Dirac semimetal and topological phase transitions in A_3Bi ($A = Na$, K, Rb), Phys. Rev. B **85**, 195320 (2012).

[2] S. M. Young, S. Zaheer, J. C. Y. Teo, C. L. Kane, E. J. Mele, and A. M. Rappe, Dirac semimetal in three dimensions, Phys. Rev. Lett. **108**, 140405 (2012).

[3] X. Wan, A. M. Turner, A. Vishwanath, and S. Y. Savrasov, Topological semimetal and Fermi-arc surface states in the electronic structure of pyrochlore iridates, Phys. Rev. B **83**, 205101 (2011).

[4] N. P. Armitage, E. J. Mele, and A. Vishwanath, Weyl and Dirac semimetals in three-dimensional solids, Rev. Mod. Phys. **90**, 015001 (2018).

[5] K. Fukushima, D. E. Kharzeev, and H. J. Warringa, Chiral magnetic effect, Phys. Rev. D **78**, 074033 (2008).

[6] D. E. Kharzeev and H. J. Warringa, Chiral magnetic conductivity, Phys. Rev. D **80**, 034028 (2009).

[7] D. E. Kharzeev, The chiral magnetic effect and anomaly-induced transport, Prog. Part. Nucl. Phys. **75**, 133 (2014).

[8] S. Kaushik, D. E. Kharzeev, and E. J. Philip, Chiral magnetic photocurrent in Dirac and Weyl materials, Phys. Rev. B **99**, 075150 (2019).

[9] D. E. Kharzeev, Topologically induced local P and CP violation in QCD × QED, Ann. Phys. (N.Y.) **325**, 205 (2010).

[10] Q. Li, D. E. Kharzeev, C. Zhang, Y. Huang, I. Pletikosić, A. V. Fedorov, R. D. Zhong, J. A. Schneeloch, G. D. Gu, and T. Valla, Chiral magnetic effect in $ZrTe_5$, Nat. Phys. **12**, 550 (2016).

[11] J. Xiong, S. K. Kushwaha, T. Liang, J. W. Krizan, M. Hirschberger, W. Wang, R. J. Cava, and N. P. Ong, Evidence for the chiral anomaly in the Dirac semimetal Na_3Bi, Science **350**, 413 (2015).

[12] C. Z. Li, L. X. Wang, H. Liu, J. Wang, Z. M. Liao, and D. P. Yu, Giant negative magnetoresistance induced by the chiral anomaly in individual Cd_3As_2 nanowires, Nat. Commun. **6**, 10137 (2015).

[13] H. Li, H. He, H. Z. Lu, H. Zhang, H. Liu, R. Ma, Z. Fan, S. Q. Shen, and J. Wang, Negative magnetoresistance in Dirac semimetal Cd_3As_2, Nat. Commun. **7**, 10301 (2016).

[14] Xiaochun Huang, Lingxiao Zhao, Yujia Long, Peipei Wang, Dong Chen, Zhanhai Yang, Hui Liang, Mianqi Xue, Hongming Weng, Zhong Fang, Xi Dai, and Genfu Chen, Observation of the chiral-anomaly-induced negative magnetoresistance: In 3D Weyl semimetal TaAs, Phys. Rev. X **5**, 031023 (2015).

[15] Y. Li, Z. Wang, P. Li, X. Yang, Z. Shen, F. Sheng, X. Li, Y. Lu, Y. Zheng, and Z. A. Xu, Negative magnetoresistance in Weyl semimetals NbAs and NbP: Intrinsic chiral anomaly and extrinsic effects, Front. Phys. **12**, 127205 (2017).

[16] Frank Arnold, Chandra Shekhar, Shu-Chun Wu, Yan Sun, Ricardo Donizeth Dos Reis, Nitesh Kumar, Marcel Naumann, Mukkattu O. Ajeesh, Marcus Schmidt, Adolfo G. Grushin, Jens H. Bardarson, Michael Baenitz, Dmitry Sokolov, Horst Borrmann, Michael Nicklas, Claudia Felser, Elena Hassinger, Binghai Yan, Negative magnetoresistance without well-defined chirality in the Weyl semimetal TaP, Nat. Commun. **7**, 11615 (2016).

[17] J. M. Ziman, *Electrons and Phonons: The Theory of Transport Phenomena in Solids* (Oxford university press, 2001).

[18] T. Liang, Q. Gibson, J. Xiong, M. Hirschberger, S. P. Koduvayur, R. J. Cava, and N. P. Ong, Evidence for massive bulk Dirac fermions in $Pb_{1-X}Sn_XSe$ from Nernst and thermopower experiments, Nat. Commun. **4**, 2696 (2013).

[19] Z. Jia, C. Li, X. Li, J. Shi, Z. Liao, D. Yu, and X. Wu, Thermoelectric signature of the chiral anomaly in Cd_3As_2, Nat. Commun. **7**, 13013 (2016).

[20] Yanan Li, Huichao Wang, Jingyue Wang, Chunming Wang, Yanzhao Liu, Jun Ge, Jingjing Niu, Wenjie Zhang, Pinyuan Wang, Ran Bi, Jinglei Zhang, Ji-Yan Dai, Jiaqiang Yan, David Mandrus, Nitin Samarth, Haizhou Lu, Xiaosong Wu, and Jian Wang, Anomalous magnetothermoelectric behavior in massive Dirac materials, Phys. Rev. B **107**, 085140 (2023).

[21] H. Chi, C. Zhang, G. Gu, D. E. Kharzeev, X. Dai, and Q. Li, Lifshitz transition mediated electronic transport anomaly in bulk $ZrTe_5$, New J. Phys. **19**, 015005 (2017).

[22] W. Zhang, P. Wang, G. Gu, X. Wu, and L. Zhang, Negative longitudinal magnetothermopower in the topological semimetal $ZrTe_5$, Phys. Rev. B **102**, 115147 (2020).

[23] P. M. Lozano, G. Cardoso, N. Aryal, D. Nevola, G. Gu, A. Tsvelik, W. Yin, and Q. Li, Anomalous Hall effect at the Lifshitz transition in $ZrTe_5$, Phys. Rev. B **106**, L081124 (2022).

[24] J. L. Zhang, C. M. Wang, C. Y. Guo, X. D. Zhu, Y. Zhang, J. Y. Yang, Y. Q. Wang, Z. Qu, L. Pi, Hai-Zhou Lu, and M. L. Tian, Anomalous thermoelectric effects of $ZrTe_5$ in and beyond the quantum limit, Phys. Rev. Lett. **123**, 196602 (2019).

[25] Y. Liu, H. Pi, K. Watanabe, T. Taniguchi, G. Gu, Q. Li, H. Weng, Q. Wu, Y. Li, and Y. Xu, Gate-tunable multiband transport in $ZrTe_5$ thin devices, Nano Lett. **23**, 5334 (2023).

[26] S. Galeski, *et al.*, Origin of the quasi-quantized Hall effect in $ZrTe_5$, Nat. Commun. **12**, 3197 (2021).

[27] F. Tang, P. Wang, M. He, M. Isobe, G. Gu, Q. Li, L. Zhang, and J. H. Smet, Two-dimensional quantum Hall effect and zero energy state in few-layer $ZrTe_5$, Nano Lett. **21**, 5998 (2021).

[28] Adrien Gourgout, Maxime Leroux, Jean-Loup Smirr, Maxime Massoudzadegan, Ricardo P. S. M. Lobo, David Vignolles, Cyril Proust, Helmuth Berger, Qiang Li, Genda Gu, Christopher C. Homes, Ana Akrap, and Benoît Fauqué, Magnetic freeze-out and anomalous Hall effect in $ZrTe_5$, npj Quantum Mater. **7**, 71 (2022).

[29] S. Galeski, H. F. Legg, R. Wawrzyńczak, T. Förster, S. Zherlitsyn, D. Gorbunov, M. Uhlarz, P. M. Lozano, Q. Li, G. D. Gu, C. Felser, J. Wosnitza, T. Meng, and J. Gooth, Signatures of a magnetic-field-induced Lifshitz transition in the ultra-quantum limit of the topological semimetal $ZrTe_5$, Nat. Commun. **13**, 7418 (2022).

[30] W. Shockley, Currents to conductors induced by a moving point charge, J. Appl. Phys. **9**, 635 (1938).

[31] J. C. W. Song and L. S. Levitov, Shockley-Ramo theorem and long-range photocurrent response in gapless materials, Phys. Rev. B **90**, 075415 (2014).

[32] Qiong Ma, Chun Hung Lui, Justin C. W. Song, Yuxuan Lin, Jian Feng Kong, Yuan Cao, Thao H. Dinh, Nityan L. Nair, Wenjing Fang, Kenji Watanabe, Takashi Taniguchi, Su-Yang Xu, Jing Kong, Tomás Palacios, Nuh Gedik, Nathaniel M. Gabor, and Pablo Jarillo-Herrero, Giant intrinsic photoresponse in pristine graphene, Nat. Nanotechnol. **14**, 145 (2019).

[33] Y. Shao, *et al.*, Nonlinear nanoelectrodynamics of a Weyl metal, Proc. Natl. Acad. Sci. U. S. A. **118**, e2116366118 (2021).

[34] H. Cao, G. Aivazian, Z. Fei, J. Ross, D. H. Cobden, and X. Xu, Photo-Nernst current in graphene, Nat. Phys. **12**, 236 (2016).

[35] Q. Ma, R. Krishna Kumar, S.-Y. Xu, F. H. L. Koppens, and J. C. W. Song, Photocurrent as a multiphysics diagnostic of quantum materials, Nat. Rev. Phys. **5**, 170 (2023).

[36] Y. Zhang, *et al.*, Electronic evidence of temperature-induced Lifshitz transition and topological nature in $ZrTe_5$, Nat. Commun. **8**, 15512 (2017).

[37] Y. Tian, N. Ghassemi, and J. H. Ross, Dirac electron behavior and NMR evidence for topological band inversion in $ZrTe_5$, Phys. Rev. B **100**, 165149 (2019).

[38] O. Shigeto, S. Takashi, and I. Masayuki, Giant resistivity anomaly in $ZrTe_5$, J. Phys. Soc. Jpn. **49**, 839 (1980).

[39] W. Knap, C. Skierbiszewski, A. Zduniak, E. Litwin-Staszewska, D. Bertho, F. Kobbi, J. L. Robert, G. E. Pikus, F. G. Pikus, S. V. Iordanskii, V. Mosser, K. Zekentes, and Y. B. Lyanda-Geller, Weak antilocalization and spin precession in quantum wells, Phys. Rev. B **53**, 3912 (1996).

[40] H. Z. Lu and S. Q. Shen, Weak antilocalization and localization in disordered and interacting Weyl semimetals, Phys. Rev. B **92**, 035203 (2015).

[41] B. Zhao, P. Cheng, H. Pan, S. Zhang, B. Wang, G. Wang, F. Xiu, and F. Song, Weak antilocalization in Cd_3As_2 thin films, Sci. Rep. **6**, 22377 (2016).

[42] T. Liang, J. Lin, Q. Gibson, T. Gao, M. Hirschberger, M. Liu, R. J. Cava, and N. P. Ong, Anomalous Nernst effect in the Dirac semimetal Cd_3As_2, Phys. Rev. Lett. **118**, 136601 (2017).